A latitudinal survey of CO, OCS, H₂O, and SO₂ in the lower atmosphere of Venus: Spectroscopic studies using VIRTIS-H

E. Marcq,[1,2] B. Bézard,[1] P. Drossart,[1] G. Piccioni,[3] J. M. Reess,[1] and F. Henry[1]

[1] The high-resolution channel ($R \simeq 2000$) of the Visible and Infrared Thermal Imaging Spectrometer (VIRTIS) instrument (VIRTIS-H) aboard Venus Express has provided numerous spectra of the nightside infrared thermal emission in the 2.3-μm window. Mixing ratios of various minor species in the $30-40$ km range could therefore be inferred using this spectral window at higher latitudes accessible to the spacecraft but which cannot be observed from Earth. The previously known enhancement in carbon monoxide (CO) toward high latitudes is confirmed and extended up to $60°$ with a mixing ratio varying from 24 ± 3 to 31 ± 2 ppmv at 36 km. Measurements of carbonyl sulfide (OCS) also agree with the previously suspected latitudinal variations that are anticorrelated with those of CO, ranging between 2.5 ± 1 and 4 ± 1 ppmv at 33 km. New constraints were also derived on the mean abundance of water vapor (H_2O, 31 ± 2 ppmv) and sulfur dioxide (SO_2, 130 ± 50 ppmv) in the probed altitude range. CO and OCS variations are interpreted as caused by large-scale vertical motions, an explanation under current testing by various chemical and dynamical modeling. In such a case, these variations may help constrain the chemical time scale of those species in the lower troposphere.

1. Introduction

[2] The discovery of Venus' nightside near infrared emission in 1983 by *Allen and Crawford* [1984] provided a new, valuable method to investigate the deep atmosphere of the planet. The physical origin of this emission was rapidly understood in the 1980s, on the basis of its physical properties and successful modeling [*Crisp et al.*, 1989; *Kamp et al.*, 1988]. The hot and deep layers of the lower atmosphere emit strong thermal radiation that can partly escape the thick atmosphere in a few narrow spectral windows thanks to the sub-Lorentzian behavior of CO_2 line shape and the weakly absorbing scattering by the H_2SO_4 particles within the overlying cloud layers. In the 2.3-μm window considered hereafter, the emission originates from the $30-40$ km altitude range (average temperature of about 500 K).

[3] Besides the imaging of the lower cloud deck whose opacity modulates the intensity of these emissions [*Carlson et al.*, 1991], the main scientific interest comes from its spectroscopic analysis. The comparison with radiative transfer synthetic models [*Bézard et al.*, 1990; *Kamp and Taylor*, 1990; *Pollack et al.*, 1993; *de Bergh et al.*, 1995] provided numerous constraints on the abundance of minor gaseous constituents. In the 2.3-μm window, carbon monoxide (CO), carbonyl sulfide (OCS), water vapor (H_2O, HDO), sulfur dioxide (SO_2) and hydrofluoric acid (HF) were detected and measured thanks to their spectral signatures. Furthermore, the spectral behaviors of CO and OCS are rich enough so that not only their mean abundance level, but also their respective vertical gradients could be derived, and were shown to be opposite by *Pollack et al.* [1993], with CO increasing with altitude as it is produced by the photochemistry of CO_2 above 60 km.

[4] The study of local compositional variations began later, in the 1990s, when *Collard et al.* [1993] noticed in the NIMS/Galileo spectra recorded during the flyby that the spatial variations of the CO band shape indicated a northern enrichment at higher latitudes of about 35%. More recently, spectra have been acquired at the NASA IRTF using the spectrometer SpeX during the quadratures that occurred since 2003. Their better spectral resolution compared to NIMS allowed us to confirm the CO northern enrichment and report a similar enrichment in the southern hemisphere, as well as a correlated depletion of OCS [*Marcq et al.*, 2005, 2006] in the portions of Venus' nightside that can be

[1]Laboratoire d'Études Spatiales et d'Instrumentation en Astrophysique, UMR8109, CNRS, Observatoire de Paris, Meudon, France.
[2]Laboratoire de Météorologie Dynamique, UMR8539, CNRS, Université Paris 6, Paris, France.
[3]Istituto di Astrofisica Spaziale e Fisica Cosmica, Istituto Nazionale di Astrofisica, Rome, Italy.

Table 1. Summary of Mentioned Science Cases

Science Case	Description
1	pericenter nadir observations
2	off-pericenter nadir observations
3	apocenter mosaic observations
5	stellar occultations
7	limb observations

observed from Earth (below 40° in latitude). A latitudinal variability of the vertical gradient of these two species in the probed layers could also be measured thanks to the high signal-to-noise ratio in the best data sample, and it appears that both gradients were steeper at higher latitudes than in the equatorial region [*Marcq et al.*, 2006]. Spatial variations in water vapor have also been sought by several observers [*Drossart et al.*, 1993] since the localized enrichment reported by *Bell et al.* [1991], which was hypothesized to be due to cloud subsidence and evaporation.

[5] Keeping in mind that CO increases and OCS decreases with increasing altitude, the latitudinal variability of CO and OCS can be qualitatively understood as being primarily caused by the global meridional dynamics. At high latitudes, downward fluxes from the Hadley cell circulation bring air depleted in OCS and enriched in CO, whereas the ascending branch of these cells has the opposite effect close to the equator. Quantitative modeling is currently progressing (Y. Yung et al., Modeling the distribution of OCS in the lower atmosphere of Venus, submitted to *Journal of Geophysical Research*, 2008; E. Marcq et al., Simulations of the latitudinal variations of CO and OCS below the clouds of Venus using a general circulation model, submitted to *Journal of Geophysical Research*, 2008). Besides the use of minor species as tracers of the deep circulation, the study of the compositional variability can also be related to the geological activity of the surface; a local enrichment in water vapor and SO_2 and a correlated modification of the D/H ratio of water may indicate an ongoing volcanic eruption [*Donahue et al.*, 1997; *Grinspoon*, 1993; *Donahue*, 1999].

[6] After more than a year of activity, the VIRTIS instrument aboard ESA's Venus Express spacecraft has provided numerous spectra from the nightside of Venus very similar to the SpeX/IRTF ones. Using very similar methods to our previous studies, we present in this paper the new constraints we have derived from these data about the spatial variations of CO, OCS and water vapor, as well as a semiquantitative interpretation of the aforementioned variations.

2. Observations

2.1. VIRTIS and the Venus Express Mission

2.1.1. Brief Overview of the Mission

[7] A detailed description of the Venus Express mission is provided by *Titov et al.* [2006a]. Here we summarize the mission characteristics relevant to this study. The orbit of the spacecraft is quasi-polar, with a periapsis located at 78°N, and highly elliptical (the distance to the surface ranging from 250 km up to 66000 km) with a 24-hour period. As a consequence of the Keplerian motion of the

probe, there is an asymmetry in the observation times for both hemispheres: the northern one is seen from a nearer vantage point, but for shorter durations.

[8] Within each 24-hour orbit, 8 hours are dedicated to communication with the Earth. The remaining 16 hours are used by the six functioning instruments (ASPERA, MAG, SPICAV-SOIR, VeRa, VIRTIS, VMC) for the various Venus-related observations (such as limb or nadir sounding, solar or stellar occultations) according to preplanned schedules named "science cases." A brief summary of the science cases mentioned in this article is available in Table 1 [from *Titov et al.*, 2006b].

2.1.2. VIRTIS-H

[9] The VIRTIS spectral imager is described in detail by *Coradini et al.* [1998]. Here we describe the characteristics of the H-channel that are relevant to our analysis. The specific optical device of the H-channel consists of an echelle grating spectrometer, and dispersion orders from 8 to 15 are focused on the detector plane. The 2.3-μm emission can be seen on three among these orders, designated as orders 5, 6 and 7. The spectral resolution of each of these spectra varies with the wavelengths, as shown on Figure 1. The spectra are then sampled on 432 discrete wavelengths for each dispersion order, although the first tens of pixels on the right side (short wavelengths) of the focal plane array usually yield smaller radiances than expected because of the low grating efficiency on the edges of the orders, thus reducing their effective spectral ranges. Another peculiarity of the array reading system that we had to take into account in our processing methods is the difference in fluxes between odd and even pixels along a given spectrum. Nevertheless, this peculiarity is partially corrected by the calibration process, yielding a few percent difference in the absolute intensities between even and odd pixels.

2.2. Quality of the Observations

2.2.1. Orbits

[10] We have currently reviewed all VIRTIS-H spectra between orbits 7 (27 April 2006) and 298 (13 February 2007). The proportion of orbits during which nightside spectra could be successfully acquired is close to 40%. This
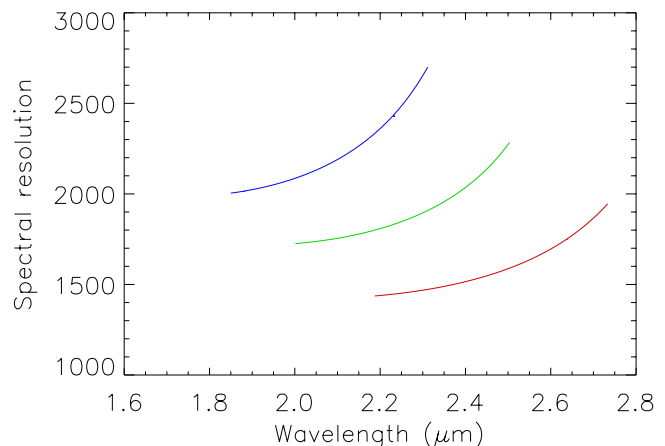
Figure 1. Spectral resolution versus wavelength for orders 5 (red), 6 (green), and 7 (blue).

Table 2. Processed Orbits

| Orbit	Number of Processed Spectra	Science Case	Latitude on Venus	Single Spectrum S/N Ratio
007	128	N/A[a]	29°S−26°S	10
024	100	1	20°S−55°N	3−10
027	35	1	20°N−60°N	8−12
033	32	7	20°N−50°N	4−8
040	50	7	0°−60°N	4−6
042	40	7	40°N−60°N	6
060	160	7	10°S−70°N	3−8
061	140	2	30°S−50°N	4−8
073	230	1	30°S−20°N	4−12
074	230	5	30°S−20°N	10−30
076	128	1	35°N−55°N	4−8
077	192	2	44°S−40°S	5
078	300	1	10°S−70°N	2−4
079	200	1	0°−70°N	4−25
082	80	1	25°N−60°N	2−6
088	80	7	30°N−70°N	4−18
095	50	2	40°N−70°N	4−8
096	1728	2	58°S−44°S	3−4
097	40	1	40°N−60°N	3
098	1664	2	55°S−28°S	3−4
100	30	2	45°N−55°N	4
102	30	2	30°N−55°N	5
103	30	5	30°N−50°N	5
104	50	2	10°N−55°N	2.5
110	2880	2	50°S−15°S	4
110	150	2	10°N−60°N	4
111	640	2	49°S−24°S	2−8
113	50	2	35°N−60°N	3
116	50	2	35°N−60°N	3
125	32	5	35°N−60°N	3
128	1400	2	60°S−45°S	4
129	320	2	11°S−50°N	4
134	1200	2	60°S−45°S	4
136	200	2	56°S−54°S	10
139	40	2	20°N−70°N	3−4
143	96	2	10°S−5°N	3
148	50	2	11°N−25°N	5
243	160	1	25°S−40°N	12
248	1100	3	43°S−40°S	10
249	150	1	0°−60°N	20
258	250	5	30°S−0°	6
277	96	1	20°S−5°S	20
284	51	2	20°S−50°N	4−10
298	200	1	10°S−40°N	4−14

[a]During insertion orbit.

proportion and the temporal distribution of these orbits are consistent with the expected requirements (VIRTIS operational and pointing to a location on the nightside). Nevertheless, a subset of these orbits (14% of the total number) show a S/N ratio significantly better than those of the typical spectra taken at similar latitudes. They are summarized in Table 2. The retrievals shown in section 3.2 have therefore been conducted on this subset.

2.2.2. Influence of the Observing Mode ("Science Case")

[11] Quite surprisingly, the periapsis observations (case 1) were not the ones which consistently yielded the best spectra. It can be understood when we consider that the limiting factor in the processing of the VIRTIS-H spectra is the signal-to-noise ratio. In order to improve it, we have to integrate signal for as long as possible: at least a couple of minutes (around 20 frames in case 1) and up to half an hour, and a few hundred spectra for off-pericenter (case 2) or apoapsis mosaic observations (case 3), when the orbital velocity is slower than for periapsis observations. Longer integration times are not suitable for a study of spatial variations, since the location on Venus of the various spectra would be blurred owing to the motion of the spacecraft. As a comment, it should be noted that even if it could theoretically be done, it would be useless to shorten the integration time to enhance the spatial resolution below roughly 30 km, since multiple scattering of the thermal emission by the cloud particles causes an intrinsic blurring of the signal over such a horizontal scale. Actually, our integration signal causes a latitudinal extension of the spectra's location over a few degrees at most (longitudinal extension can be neglected owing to the quasi-polar orbital motion), thus enabling an integrated S/N ratio around 100 (individual spectra's S/N ratios are given in Table 2).

[12] Considering this trade-off between spatial resolution and signal-to-noise ratio, it appears that case 1 observations are well suited to low-latitude regions, where the signal is strong enough to cope with the moderate integration durations available in this science case owing to the high orbital velocity. On the other hand, midlatitudinal to high-latitudinal
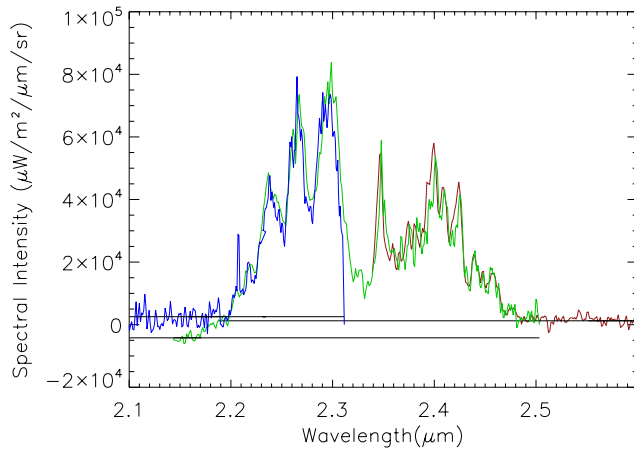
Figure 2. Superimposition of averaged nightside spectra of the same location on orders 5 (red), 6 (green), and 7 (blue) and their respective zero level. Note also the difference of spectral resolution between the various orders, in agreement with Figure 1.

regions require a slower orbital velocity which can ensure a longer integration in spite of an increased distance. This explains why high-latitude regions have been mostly successfully observed during science cases 2, 5 or even 3.

2.3. Comparison with Similar Earth-Based Spectra

[13] Sets of very similar spectra in terms of spectral range (1.92–2.52 μm) and resolution (R = 2000) have been acquired since 2003 using SpeX/IRTF by *Marcq et al.* [2005]. These observation campaigns were intended as a benchmark for the methods used hereafter, so that a comparison between these previous studies [*Marcq et al.*, 2005, 2006] and the present one is very interesting. However there are some differences between both data sets that should be highlighted.

2.3.1. Spatial and Temporal Coverage

[14] First of all, the spatial and temporal coverage is of course much better for VIRTIS, a dedicated instrument aboard a space probe orbiting Venus, than for the ground-based observations. From Earth, the nightside of Venus can be successfully observed only for a few weeks between inferior conjunction and maximal elongation. This period of favorable observing geometry occurs only twice in every 19.2 months. In contrast, VIRTIS has been providing spectra of the nightside of Venus on a regular basis (40% of the orbits on average) since April 2004 and will continue until at least the end of the extended mission in 2009. Another interesting feature of the Venus Express observations is that the quasi-polar orbit enables the observation of northern and southern circumpolar regions which are otherwise unreachable; the farthest observations with respect to the Venusian equator using SpeX could only reach 40 degrees of latitude.

2.3.2. Preliminary Processing

[15] Another major advantage of space-based observations is the absence of any sunlight reflected from the dayside in virtually all nightside spectra, thanks to the apparent size of Venus as seen from the spacecraft. For SpeX observations, the much smaller angular diameter of

Venus and the fact that a significant portion of the visible Venusian disk is illuminated near maximal elongation can lead to a strong scattering of the much brighter light from the solar illuminated portion of the planet onto the night-side, reducing the attainable S/N. The removal of the diffused component is a significant step in the processing and a major source of uncertainty for the retrievals of *Marcq et al.* [2005] and *Marcq et al.* [2006]: it prevented the observation of the nightside hemisphere close to the termi-nator, thus contributing to the narrowness of the latitudinal range of Earth-based observations.

[16] Nevertheless, some processing is also needed for VIRTIS-H spectra, since the 2.3 μm window is covered by 3 different orders of dispersion that should agree on the actual intensity observed within their common spectral ranges. A typical superimposition is shown on Figure 2 for orders 5, 6 and 7. The differences on the actual value of the zero-intensity level are clearly visible between order 6 on one hand and orders 5 and 7 on the other hand. In the subsequent processing, the actual zero level for order 6 is computed from the zero levels measured on the orders 5 and 7, whose mutual agreement despite being on opposite sides of the 2.3-μm window make more trustworthy than order 6's short-wavelength zero level.

[17] As a last comment, Earth-based observations must also be corrected for the spectral signature of the terrestrial atmosphere, especially for water vapor which is much more abundant on Earth than on Venus. Such a concern is absent for VIRTIS observations, which makes them more reliable, especially for water vapor retrievals.

2.3.3. Signal-to-Noise Ratio

[18] One major asset of Earth-based observations com-pared to VIRTIS-H ones is their quality. The longer inte-gration time and especially the much greater light collecting area available more than compensate for the much greater distance between the instrument and Venus. A typical individual VIRTIS-H spectrum in a low-latitude to mid-latitude region has a S/N ratio of between 5 and 10. Averaging over a few tens of spectra improves this ratio to about 50, at the expense of a having a spatial precision roughly equivalent to that of SpeX observations with a seeing of about 1 arcsec. SpeX spectra which are compa-rable in terms of integration time, location on Venus and latitudinal extension show an S/N ratio of 100 or higher. Thus, rather than supplementing Earth-based observations, VIRTIS provides a long-needed complementary spatial and temporal coverage of nightside deep atmosphere.

3. Retrievals

3.1. Algorithms

3.1.1. Synthetic Model

[19] The forward synthetic model that we use is exactly the same as described by *Marcq et al.* [2006]. A typical fit is shown on Figure 3.

[20] A major flaw of all radiative transfer models used to investigate the 2.3-μm window is the poor fit in the CO_2 dominated spectral domain between 2.2 and 2.3 μm. There-fore, we have tried the new CDSD-750 database for CO_2, suited for high-temperature calculations as encountered in the probed altitude region. Unfortunately, the fit we obtained was worse compared to the same model using the
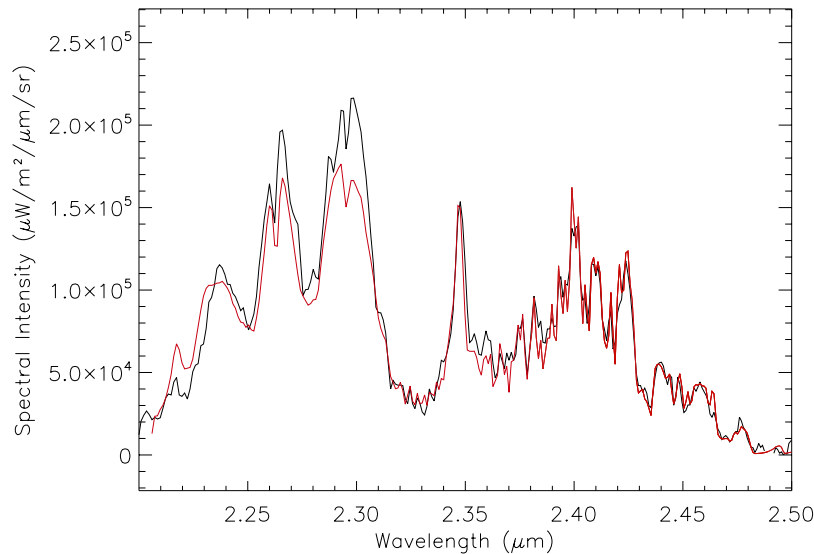
Figure 3. Comparison in the 2.2–2.5 μm interval of a good quality order 6 spectrum (from orbit 277, in black) with the synthetic model. The relatively poor agreement at wavelengths shortward of 2.3 μm is due to the poor knowledge of CO_2 opacity.

older HITEMP database, whether a continuum absorption for CO_2 was considered or not. So we discarded the CDSD-750 database, reverted to the HITEMP database and kept the continuum absorption of CO_2 to the usual constant value of 3.5×10^{-8} cm^{-1}.amagat^{-2} throughout the window [*Pollack et al.*, 1993; *Marcq et al.*, 2006], owing to the lack of experimental measurements at the relevant pressures and temperatures.

[21] An update of the temperature profile that we consider in all of our simulations has also been tried from the older mean VIRA profile [*Seiff*, 1983] to the newer VIRA-2 [*Moroz and Zasova*, 1997]. A comparison between the two profiles in the altitude range where the emission originates from (30 to 40 km) showed very little difference, especially for the vertical gradient dT/dz. This latter could have been a concern since altering dT/dz distorts the simulated spectra in almost the same way as a change in CO abundance; it affects the relative brightness temperature of neighboring atmospheric layers where CO mixing ratio differs. On the contrary, changing the mean temperature of the 30–40 km region while maintaining the temperature gradient produces almost no shape distortion of the spectra, but merely alters the integrated flux in the whole window, as expected. As far as we are concerned, the differences were too weak to justify a change of our temperature profile.

[22] Still, the assumption of a horizontally uniform temperature profile could be invalid in the polar regions (above 60° in latitude), where some variability of $T(z)$ is expected even in the lower atmosphere [*Pätzold et al.*, 2007]. But these regions yield a too weak signal in VIRTIS-H to be studied, so that we maintained this assumption. It is also worth noting that the weaker fluxes of the polar region are caused by a thicker lower cloud cover, whose modal distribution of aerosols is poorly known. A proper modeling of nightside polar spectra would therefore require a good understanding of both temperature profile and vertical

and modal distribution of cloud particles, which are both difficult to assess yet.

[23] Finally, the synthetic spectra were sampled and convolved according to the instrumental function to allow straightforward comparison between synthetic and observed spectra. The instrumental functions differ for orders 5 and 6, and their width and shape vary with wavelength in a complex way.

3.1.2. One-Parameter Retrieval

[24] The algorithm is based on a simple calculation of the residuals between an observed spectrum and various sets of precomputed synthetic spectra of various prescribed atmospheric parameters (e.g., vertical profiles of minor constituents, cloud opacity) within a few specific spectral intervals. This algorithm is almost exactly similar to the one described in section 4.1.1. by *Marcq et al.* [2006], except for some minor adaptations due to the differences between VIRTIS-H and SpeX.

[25] Actually, besides the different determination of the true zero level (see 2.3.2) and, more generally, the completely different preprocessing, especially regarding diffused sunlight removal for SpeX, the key differences come from the fact that VIRTIS-H nightside spectra are available on two dispersion orders (5 and 6; order 7 was only used for zero-level determination since it does not cover the minor species absorption bands). Furthermore, the totality of the 2.3-μm window is only available on order 6, as can be seen on Figure 2: the 2.2-2.3 μm interval is not accurately rendered in order 5. From these considerations, the following adaptations were required:

[26] 1. The former version of the algorithm used the same spectral interval to compute the free-scaling parameter a_i (designed to have the best possible agreement between a given synthetic spectrum S_i and the observed spectrum E) and to compute the residuals between E and S_i. Owing to the lack of coverage for order 5, the algorithm is now able to use spectral intervals that are distinct for these two uses, the
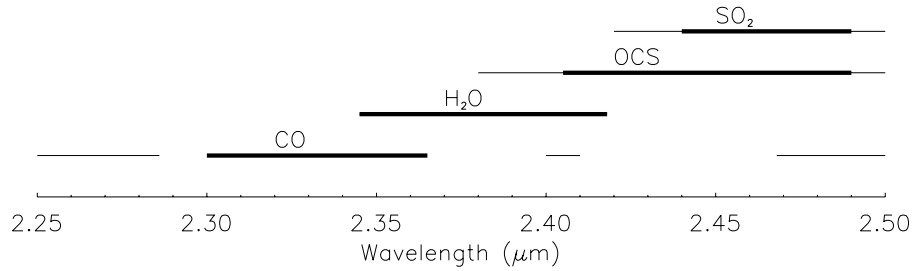
Figure 4. Spectral intervals used by our algorithm for the various species. The thick lines correspond to the residual computation intervals, whereas the whole lines (thin and thick) correspond to the scaling parameter determination intervals.

scaling interval typically being a superset of the residual estimation interval. The actual values, which can differ from order to order, are shown on Figure 4.

[27] 2. Orders 5 and 6 of VIRTIS-H overlap between 2.3 and 2.5 μm. Although the analysis on both orders is done separately since they yield two distinct spectra of the same location, the estimates are considered as two independent measurements of the same spectrum: the resulting estimation e and its uncertainty σ are given by the following formulæ: $e = \frac{\sigma_6^2 e_5 + \sigma_5^2 e_6}{\sigma_6^2 + \sigma_5^2}$ and $\sigma = \frac{\sigma_5 \sigma_6}{\sqrt{\sigma_5^2 + \sigma_6^2}}$, where the subscripts 5 and 6 refer to the considered order. To ensure the consistency of such a combination, the retrievals were dismissed if their maximal normalized probability density, given by $\exp[-\frac{(e_6 - e_5)^2}{\sigma_6^2 + \sigma_5^2}]$, was inferior to a threshold depending on the species, usually between 0.8 and 0.9. Note that coadding spectra from orders 5 and 6 would not make sense since their spectral resolution differ on their common wavelength range.

3.1.3. Strategy for Retrieving Gaseous Profiles

[28] The global retrieval strategy is mostly unchanged since *Marcq et al.* [2006], where the 2.3-μm window was studied sequentially from the shorter wavelengths to the longer ones. The spectral intervals used for the retrievals of these three species are shown on Figure 4. Note that wavelengths less than 2.35 μm could not be used for order 5-based retrievals, since the instrument underestimates the intensity at these wavelengths for this order.

3.1.3.1. Carbon Monoxide Retrieval

[29] The CO absorption band centered at 2.33 μm cannot be properly observed on order 5, so that only order 6 can be used for the retrievals. Spectral distortions due to the variation of the lower cloud opacity between the various spectra are taken into account as by *Marcq et al.* [2006] by first measuring the cloud opacity using integrated spectral radiance between 2.2 and 2.5 μm and then accordingly interpolating the synthetic spectra to the measured opacity. The considered set of CO vertical profiles are all proportional to the standard VIRA-2 profile.

3.1.3.2. Water Vapor Retrieval

[30] Spectra from both orders 5 and 6 can be used for this species. Variations of lower cloud opacity, which affect spectral radiance in the whole window, and carbon monoxide, measured at the previous step and whose absorption band overlaps the water absorption band, are taken into account in the same way as previously stated. The set of synthetic profiles are here also proportional to the standard VIRA-2

profile, with no attempt to explore various D/H ratios at this stage.

3.1.3.3. Carbonyl Sulfide Retrieval

[31] Spectra from orders 5 and 6 were also processed for the retrievals. Spectral overlapping with water vapor and carbon monoxide requires that the variations of these two species are taken into account, not to mention the consideration of cloud opacity variations here also. The set of considered synthetic profiles are various vertical translations of the standard VIRA-2 profile.

3.1.3.4. Sulfur Dioxide Retrieval

[32] Its spectral signature being very narrow, sulfur dioxide retrievals are performed tentatively with a very low accuracy, using orders 5 and 6. Variations of carbonyl sulfide, water vapor and lower cloud opacity are taken into account, with the SO_2 profiles assumed to be vertically uniform.

3.2. Results

3.2.1. CO

[33] The mixing ratio of carbon monoxide at 36 km inferred at various locations is plotted on Figure 5. The minimal value of 24 ± 3 ppmv appears to be slightly off the equator, between 0° and 20°S. Its abundance then rises symmetrically with respect to this minimum toward higher latitudes, reaching 31 ± 2 ppmv at 60°S and between 30 and
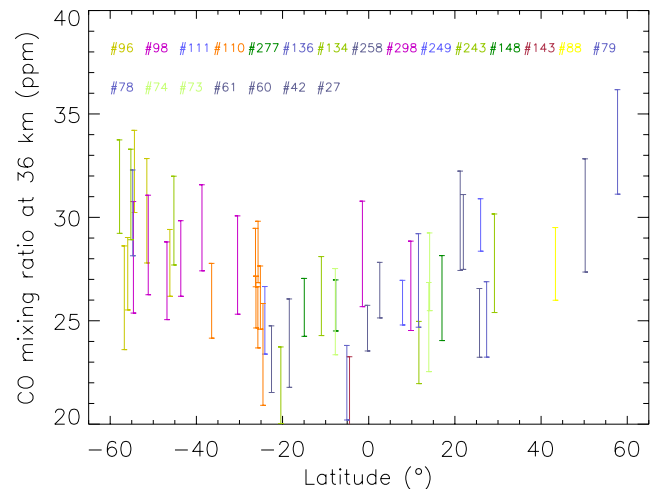
Figure 5. Variations of the CO abundance at 36 km according to various VIRTIS-H spectra (orbits shown in various colors). Error bars stand for 1-σ uncertainty levels.
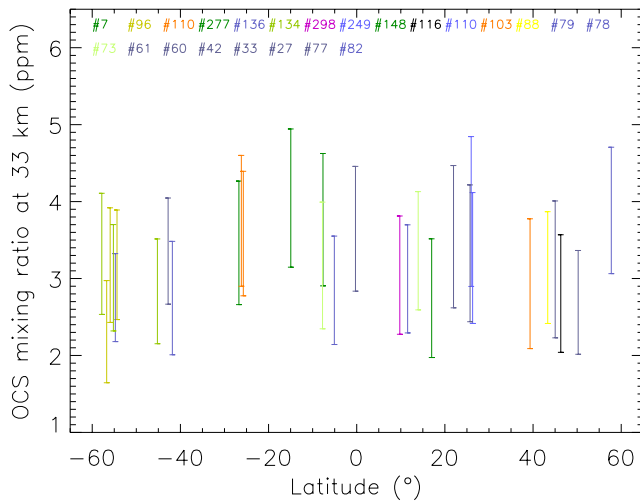
Figure 6. Variations of the OCS abundance at 33 km according to various VIRTIS-H spectra (orbits shown in various colors). Error bars stand for 1-σ uncertainty levels.

40 ppm at 60°N, where the coverage is not dense enough to ensure as much accuracy as in its southern counterpart. The dispersion of the measurements suggests some longitudinal and/or temporal variability within less than the 300-day interval during which the processed spectra have been acquired, although never exceeding 20% of the zonal mean value nor the pole-to-equator gradient.

3.2.2. OCS

[34] Carbonyl sulfide latitudinal variations are shown on Figure 6. These variations appear to be anticorrelated to those of carbon monoxide, showing a maximal value of 4 ± 1 ppmv between 20°S and the equator, which was also the latitude where CO was minimal; the asymmetry of CO and OCS variations with respect to the equator could be related to the presence of high-elevation landmasses (namely, Aphrodite Terra, which is centered around 10° S) through the perturbations they cause to the general circulation. The minimum value of 2.5 ± 1 ppmv is reached near 60°S. The relative uncertainty on these retrievals is quite high, higher than what the S/N value or the accuracy of the fitting could account for, and such that we cannot dismiss a latitude-independent mixing ratio between 3 and 3.5 ppm. Our current interpretation of this poor precision is related to the choice of the 1-D vertical synthetic profile set mentioned in section 3.1.3, which implies a univocal relation between mean abundance and vertical gradient. This relation prevents the exploration of the whole 2-D parameter space to which spectra are sensitive (i.e., vertical gradient and, independently, mean abundance in the 30–36 km range). The explored subset is probably out of the optimal fit region since the dispersion of measurements is consistently inferior to the 1-σ error bars, which points out that statistical noise is not the only source of discrepancy between synthetic and observed spectra. The same concern was raised by *Marcq et al.* [2006], and was solved by enabling the vertical gradient and the abundance to be retrieved separately. Such a study requires very high S/N ratio, and is therefore still in progress for the best VIRTIS-H spectra currently available.

3.2.3. H2O

[35] As concerns water vapor, no similar latitudinal trend could be observed on our results shown on Figure 7. Nevertheless, the combination of order 5 and 6 retrievals has enabled us to enhance the accuracy on its mean value significantly: 31 ± 2 ppmv between 30 and 40 km. Some temporal and/or longitudinal variability may also be possible with slightly drier conditions (29 ± 1 ppm) past 20°N, but this departure with the mean value is not significant: we have no evidence for any variations within this data set.

3.2.4. SO2

[36] Sulfur dioxide measurements could not reach a high accuracy considering the narrowness of its spectral band on the long-wavelength edge of the 2.3-μm spectral window, so that no latitudinal variation could be detected (see Figure 8). The assumption that the mixing ratio is uniform yields a mean mixing ratio of 130 ± 50 ppmv.

3.3. Comparison with other Spectroscopic Studies

3.3.1. Lower-Resolution Spectra

[37] Observations at lower spectral resolution could constrain with a similar accuracy the species with the most prominent band in the whole 2.3-μm window, namely, CO. H2O and OCS retrievals are currently in progress at a lesser precision compared to VIRTIS-H retrievals. Nevertheless, these studies require less signal to work on, so their horizontal coverage is substantially larger. The observations of *Collard et al.* [1993] using NIMS/Galileo were the first of this kind, and pointed to a northern enrichment in CO of 35 ± 15% from the equator to 47°N, in a good agreement with ours (30 ± 15% in the same latitudinal range). More recently, *Tsang et al.* [2008] has used VIRTIS-M spectra to map the CO abundance over large portions of the night hemisphere, and their conclusions about the latitudinal trends for CO corroborate ours in both hemispheres: from 23 ± 2 ppm near the equator to 32 ± 2 ppm at 35 km around 60°–70°.

3.3.2. Similar Resolution or Higher-Resolution Spectra

[38] Spectra at a resolution similar or higher than ours in the 2.3-μm spectral window have been acquired and pro-
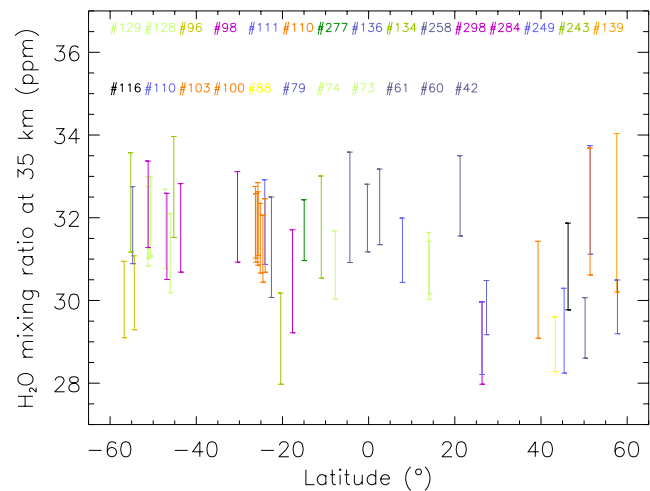
Figure 7. Variations of the water vapor at 33 km according to various VIRTIS-H spectra (orbits shown in various colors). Error bars stand for 1-σ uncertainty levels.
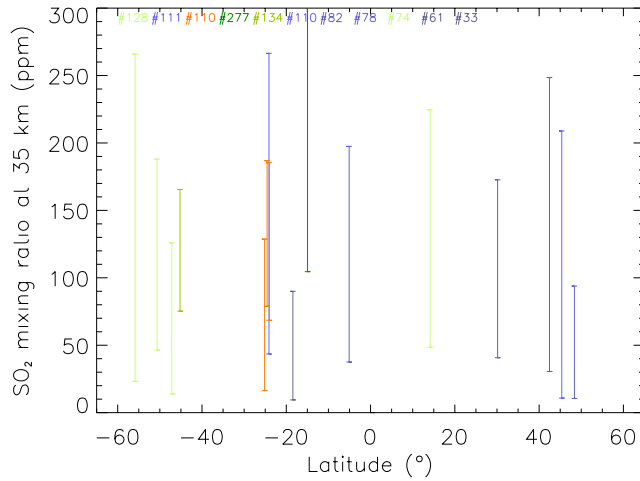
Figure 8. Variations of the sulfur dioxide at 35 km according to various VIRTIS-H spectra (orbits shown in various colors). Error bars stand for 1-σ uncertainty levels.

cessed before, but focused first on obtaining horizontally averaged spectra rather than studying their spatial variations. Comparisons are nevertheless useful, and agree with our results. The mean values of the CO mixing ratio at 36 km given by *Pollack et al.* [1993], *Bézard et al.* [1990] and *Taylor et al.* [1997] range between 20 and 30 ppm, consistent with our own measurements. Using the same spectra, OCS and SO_2 were also constrained, and respectively found to be 4.4 ± 1 ppm at 33 km (OCS [*Pollack et al.*, 1993]) and 130 ± 40 ppm between 30 and 40 km (SO_2 [*Bézard et al.*, 1993]). These determinations are also in full agreement with our own averages. The mean H_2O mixing ratio between 30 and 40 km was found using high-resolution ($R \sim 20000$) CFHT spectra in the 1.74 and 2.3-μm windows by *de Bergh et al.* [1995] to be 30 ± 10 ppm, which is also fully compatible with ours. In contrast, the lower estimate of 26 ± 4 ppm found by *Marcq et al.* [2006] is possibly due to contamination by terrestrial water vapor: the mean abundance is probably closer to 30 ppmv than to 26.

[39] More recently, latitudinal studies in this spectral window were conducted using SpeX/IRTF spectra [*Marcq et al.*, 2005, 2006] in order to prepare the processing of VIRTIS-H spectra. These results also agree with ours, at least in the latitude interval that can be observed from Earth: CO was found to vary between 26.5 ± 0.5 ppm (36 km) near 40°S and 23.75 ± 0.75 ppm near the equator, which matches our results. OCS variations were similarly anticorrelated with CO, although quantitative comparisons are harder considering the large vertical gradient of OCS in this region since their results are given at a different altitude of reference (36 km instead of 33).

3.4. Dynamical Interpretations

3.4.1. Qualitative Interpretation

[40] The current interpretation of the anticorrelated variations of CO and OCS relies upon our knowledge of the global-scale circulation, especially vertical motions. It is known [*Pollack et al.*, 1993; *Marcq et al.*, 2006] that in the 30–40 km altitude range, CO mixing ratio increases with height whereas OCS decreases. These observed vertical gradients are also predicted by most chemical models

[*Krasnopolsky*, 2007; *Krasnopolsky and Pollack*, 1994]: CO is produced by photo-dissociation of CO_2 by UV radiation above the clouds and consumed in the lower atmosphere as a reducing agent, whereas OCS is produced at ground level by reactions involving pyrite, CO and CO_2 whereas it is strongly oxidized by SO_3 (coming from the evaporation of H_2SO_4 at the lower cloud floor). The Hadley-cell vertical circulation of Venus causes upward motion in the equatorial region (due to solar heating) and downward motion at higher latitudes; most global circulation models (GCMs) predict the peak of downward velocity around 60° (S. Lebonnois et al., Superrotation of Venus' atmosphere analysed with a full General Circulation Model, manuscript in preparation, 2008). Therefore, there is a tendency to deplete the CO mixing ratio around the equator (and increase that of OCS, which is more abundant at lower levels) whereas the trends are opposite at higher latitudes, which is precisely the observed pattern for CO and OCS. We can also note that the other measured species (H_2O and SO_2), which do not exhibit latitudinal variations, have no detectable vertical gradient either.

3.4.2. Estimate of Typical Relaxation Times

[41] If the explanation given above is true, we can estimate the order of magnitude of the chemical relaxation time toward thermochemical equilibrium profiles for CO and OCS, assuming that the latitudinal contrasts we observe are caused only by the large-scale vertical motions. This coarse approach neglects other phenomena such as diffusion, and is very simplistic as for the chemical modeling, so it cannot yield more than order-of-magnitude estimates of the chemical time scale.

[42] The advected net flux of a tracer whose mixing ratio is q is given in a 1-D vertical model by $-\vec{\nabla} \cdot (q\vec{v}) = -w \frac{dq}{dz} - \frac{dw}{dz} q$, where $\vec{v}$ stands for the wind speed vector, w for the vertical wind velocity and z for the altitude. Neglecting the variation of w between 30 and 40 km, this flux is in balance with the chemical relaxation $\frac{\partial q(z)}{\partial t}|_{chem} = -\frac{q(z)-q_0(z)}{\tau}$ where τ stands for the characteristic time and $q_0(z)$ the expected vertical profile in the absence of any dynamical perturbation. In a stationary regime, this yields

$$\tau = \frac{q_0 - q}{w \frac{dq}{dz}}$$

$q - q_0$ is typically around a few ppm, $|dq/dz|$ about 1 ppm/km for CO and OCS [*Pollack et al.*, 1993; *Taylor et al.*, 1997; *Marcq et al.*, 2006] and GCMs predict typical velocities below 1 mm/s. This gives for both species characteristic times $\tau \sim 10^6 - 10^7$, s in order to allow the formation of the equator-to-pole gradients in CO and OCS seen here. We would like to stress that this value is not related to a definite chemical process, but should merely be seen as a threshold: a faster chemistry (with a smaller τ) would not allow enough time for the vertical circulation to establish the latitudinal contrasts described in section 3.2. Other characteristic times could be expressed regarding other processes (e.g., horizontal circulation, eddy diffusion), but a more detailed description is beyond the scope of this paper.

3.4.3. Quantitative Studies in Progress

[43] To progress further in the interpretation of CO and OCS variations, a number of modeling efforts are currently

in progress. The one from Yung et al. (submitted manuscript, 2008) focuses on OCS and adopts an accurate chemical scheme embedded in a 2-D circulation model, whereas Marcq et al. (manuscript in preparation, 2008) models both CO and OCS-type tracers with a simple relaxation scheme within a full 3-D radiatively consistent GCM. The results of these two models can be found in the above-quoted papers.

4. Conclusion

[44] First of all, these results stress the complementary role of VIRTIS-M and VIRTIS-H channels of Venus Express, the precision of abundance retrievals and the number of species being the main assets of VIRTIS-H in this field whereas the CO mapping capabilities of VIRTIS-M over large extents on the Venus nightside are not accessible here. We have also significantly improved the accuracy of water vapor retrievals thanks to the availability of two spectral orders over the 2.3-μm spectral window. Even using a single order, CO variations were confirmed and validated up to $60°$ in latitude for both hemispheres, still fully compatible with previous estimates by *Collard et al.* [1993] and *Marcq et al.* [2005] ($30 \pm 15\%$). Anticorrelated OCS variations first noticed from Earth were also tentatively confirmed and extended in the same latitudinal range, though the relatively poor accuracy of the retrievals cannot rule out a constant value; the accuracy of the OCS retrievals should greatly benefit from a more detailed study with OCS abundance and vertical gradient being derived separately as it was the case for *Marcq et al.* [2006].

[45] With the oncoming extended phase of Venus Express, the prospective of future observations are very good. Exploration of high-latitude region (beyond $60°$) could be possible thanks to the implementation of new science cases (enabling the tracking of a specific location during longer times), although such a study would probably require new additional information (better knowledge of possible horizontal variations of the $T(p)$ profile, modal and vertical distribution of aerosol particles). Supportive studies from space and/or Earth in the other spectral windows could also help in constraining the vertical profiles of several minor species at different altitudes, especially H_2O.

[46] The first results of coupled dynamical-chemical simulations are also expected to improve significantly our understanding of the chemistry below the clouds of Venus, especially regarding the relative time scales of various dynamical and chemical phenomena. Observational constraints provided by the present paper are also of paramount interest for developing and improving such complex coupled simulations.

References

Allen, D. A., and J. W. Crawford (1984), Cloud structure on the dark side of Venus, *Nature*, *307*, 222–224.

Bell, J. F., P. G. Lucey, T. A. Ozoroski, W. M. Sinton, and D. Crisp (1991), Spectroscopic observations of bright and dark emission features on the night side of Venus, *Science*, *252*, 1293–1296.

Bézard, B., C. de Bergh, D. Crisp, and J.-P. Maillard (1990), The deep atmosphere of Venus revealed by high-resolution nightside spectra, *Nature*, *345*, 508–511, doi:10.1038/345508a0.

Bézard, B., C. de Bergh, B. Fegley, J.-P. Maillard, D. Crisp, T. Owen, J. B. Pollack, and D. Grinspoon (1993), The abundance of sulfur dioxide below the clouds of Venus, *Geophys. Res. Lett.*, *20*, 1587–1590.

Carlson, R. W., et al. (1991), Galileo infrared imaging spectroscopy measurements at Venus, *Science*, *253*, 1541–1548.

Collard, A. D., et al. (1993), Latitudinal distribution of carbon monoxide in the deep atmosphere of Venus, *Planet. Space Sci.*, *41*, 487–494, doi:10.1016/0032-0633(93)90033-X.

Coradini, A., et al. (1998), VIRTIS: An imaging spectrometer for the ROSETTA mission, *Planet. Space Sci.*, *46*, 1291–1304.

Crisp, D., W. M. Sinton, K.-W. Hodapp, B. Ragent, F. Gerbault, and J. H. Goebel (1989), The nature of the near-infrared features on the Venus night side, *Science*, *246*, 506–509.

de Bergh, C., B. Bézard, D. Crisp, J. P. Maillard, T. Owen, J. Pollack, and D. Grinspoon (1995), Water in the deep atmosphere of Venus from high-resolution spectra of the night side, *Adv. Space Res.*, *15*, 79–88.

Donahue, T. M. (1999), New analysis of hydrogen and deuterium escape from Venus, *Icarus*, *141*, 226–235, doi:10.1006/icar.1999.6186.

Donahue, T. M., D. H. Grinspoon, R. E. Hartle, and R. R. Hodges (1997), Ion/neutral escape of hydrogen and deuterium: Evolution of water, in *Venus II: Geology, Geophysics, Atmosphere, and Solar Wind Environment*, edited by S. W. Bougher, D. M. Hunten, and R. J. Philips, pp. 385–414, Univ. of Ariz. Press, Tucson.

Drossart, P., et al. (1993), Search for spatial variations of the H_2O abundance in the lower atmosphere of Venus from NIMS-Galileo, *Planet. Space Sci.*, *41*, 495–504, doi: 10.1016/0032-0633(93)90032-W.

Grinspoon, D. H. (1993), Implications of the high D/H ratio for the sources of water in Venus' atmosphere, *Nature*, *363*, 428–431, doi:10.1038/363428a0.

Kamp, L. W., and F. W. Taylor (1990), Radiative-transfer models of the night side of Venus, *Icarus*, *86*, 510–529, doi: 10.1016/0019-1035(90)90231-W.

Kamp, L. W., F. W. Taylor, and S. B. Calcutt (1988), Structure of Venus's atmosphere from modelling of night-side infrared spectra, *Nature*, *336*, 360–362, doi:10.1038/336360a0.

Krasnopolsky, V. A. (2007), Chemical kinetic model for the lower atmosphere of Venus, *Icarus*, *191*, 25–37, doi:10.1016/j.icarus.2007.04.028.

Krasnopolsky, V. A., and J. B. Pollack (1994), H_2O-H_2SO_4 system in Venus' clouds and OCS, CO, and H_2SO_4 profiles in Venus' troposphere, *Icarus*, *109*, 58–78, doi:10.1006/icar.1994.1077.

Marcq, E., B. Bézard, T. Encrenaz, and M. Birlan (2005), Latitudinal variations of CO and OCS in the lower atmosphere of Venus from near-infrared nightside spectro-imaging, *Icarus*, *179*, 375–386, doi: 10.1016/j.icarus.2005.06.018.

Marcq, E., T. Encrenaz, B. Bézard, and M. Birlan (2006), Remote sensing of Venus' lower atmosphere from ground-based IR spectroscopy: Latitudinal and vertical distribution of minor species, *Planet. Space Sci.*, *54*, 1360–1370, doi:10.1016/j.pss.2006.04.024.

Moroz, V. I., and L. V. Zasova (1997), VIRA-2: A review of inputs for updating the Venus International Reference Atmosphere, *Adv. Space Res.*, *19*, 1191–1201.

Pätzold, M., et al. (2007), The structure of Venus' middle atmosphere and ionosphere, *Nature*, *450*, 657–660, doi:10.1038/nature06239.

Pollack, J. B., et al. (1993), Near-infrared light from Venus' nightside-A spectroscopic analysis, *Icarus*, *103*, 1–42, doi:10.1006/icar.1993.1055.

Seiff, A. (1983), Thermal structure of the atmosphere of Venus, in *Venus*, edited by S. W. Bougher, D. M. Hunten, and R. S. Phillips, pp. 215–279, Univ. of Ariz. Press, Tucson.

Taylor, F. W., D. Crisp, and B. Bézard (1997), Near-infrared sounding of the lower atmosphere of Venus, in *Venus II: Geology, Geophysics, Atmosphere, and Solar Wind Environment*, edited by S. W. Bougher, D. M. Hunten, and R. J. Philips, pp. 325–351, Univ. of Ariz. Press, Tucson.

Titov, D. V., et al. (2006a), Venus Express: Scientific goals, instrumentation, and scenario of the mission, *Cosmic Res.*, *44*, 334–348, doi:10.1134/S0010952506040071.

Titov, D. V., et al. (2006b), Venus Express science planning, *Planet. Space Sci.*, *54*, 1279–1297, doi:10.1016/j.pss.2006.04.017.

Tsang, C. C. C., et al. (2008), Tropospheric carbon monoxide concentrations and variability on Venus from Venus Express/VIRTIS-M observations, *J. Geophys. Res.*, doi:10.1029/2008JE003089, in press.

————————
B. Bézard, P. Drossart, F. Henry, E. Marcq, and J. M. Reess, Laboratoire d'Études Spatiales et d'Instrumentation en Astrophysique, UMR8109, CNRS, Observatoire de Paris, 5 place Juleps Janssen, F-92195 Meudon, France. (emmanuel.marcq@obspm.fr)

G. Piccioni, Istituto di Astrofisica Spaziale e Fisica Cosmica, Istituto Nazionale di Astrofisica, Via Fosso del Cavaliere 100, I-00133 Roma, Italy.